Abdel-Wahab *et al.*
Journal of Electrical Systems and Inf Technol (2020) 7:8
https://doi.org/10.1186/s43067-020-00016-5

Journal of Electrical Systems and Information Technology

RESEARCH Open Access

Dynamic investigation of Georges phenomenon related to three-phase wound-rotor induction motor

R. R. Abdel-Wahab, T. M. Abdo and H. H. Hanafy*

*Correspondence:
hanafy_hassan@hotmail.com
Electrical Power Engineering Department, Faculty of Engineering, Cairo University, Giza 12613, Egypt

Abstract

The aim of this paper is to analyze the performance of a three-phase wound-rotor induction motor (WRIM) under rotor windings asymmetry. The dynamic performance of the WRIM under healthy and rotor windings asymmetry with one-open-phase fault conditions is analyzed using a dynamic model in the ABC frame. Under opening one phase of the rotor windings, the WRIM suffers from operation at a speed near to the half of its synchronous speed, which is known as the Georges phenomenon. The behavior of the WRIM is simulated and investigated experimentally under faulty conditions for four different possible connections of rotor windings. The stator and rotor currents are analyzed using fast Fourier transformation technique to identify the fault signatures. The results prove that under opening one phase of the rotor windings the WRIM suffers from pulsating electromagnetic torque, high oscillatory stator currents and high unbalanced rotor currents. Also the results prove that the performance of the motor under rotor windings asymmetry conditions and the occurrence of Georges phenomenon depend on the type of connection of the rotor windings and fault location. Therefore, the authors suggest a special delta connection for the rotor winding to reduce the effects of this phenomenon. The simulation and experimental results show good agreement and prove the validity of the suggested delta connection.

Keywords: Wound-rotor induction motor, Rotor windings asymmetry, Open-phase fault, Georges phenomenon

Introduction

The squirrel cage induction motors have dominated the industry due to their well-known advantages, but in some application wound-rotor induction motor (WRIM) is still more used. The capability of the large WRIMs in developing a high starting torque at low starting currents by the means of adding external resistances in series with the rotor windings makes them ideal for some applications. Besides limiting the starting current, this resistance can also be used in controlling the motor speed. These advantages make the WRIMs suitable for large power industrial application such as cranes, pumps, conveyors and hoists [1].

Asymmetrical operation of induction machine results in unbalanced air gap flux, consequently unbalanced supply currents, increased losses, increased torque pulsations

and decreased average torque. Windings, magnetic circuit and motor mechanical system (mainly bearing failures) faults are the three main categories of faults of induction motors [7]. According to a survey [18] more than 36% of motor failures are related to the stator windings insulation. Turn-to-turn, coil-to-coil, line-to-line, line-to-ground and single or multi-phase windings open circuit faults are considered the main categories of stator windings faults. Turn-to-turn has been considered the most challenging one since the other types of failures are usually a consequence of turn-to-turn faults [15]. Rotor asymmetries are one of the most critical failures in induction machines. Although these faults do not cause an immediate collapse of the machine, they progressively degenerate, leading to an irreversible failure, unless condition monitoring is applied [4]. In [13], a method to discriminate between different faults in the stator and rotor windings of wound-rotor induction machines was presented. The proposed diagnostic method was based on the combination of FFT and discrete wavelet transform (DWT) applied on the rotor currents of wound-rotor induction machines. The magnetic equivalent circuit (MEC) model has been used to simulate machine performances under different winding fault conditions with Matlab/Simulink software.

In [12], winding inter-turn short circuit fault conditions in the stator and rotor sides was studied using a complete MEC. It was demonstrated that the currents through inter-turn shorted link are different in stator and rotor windings of WRIMs. The current also depends on the number of short circuit turns and the load level. In [10], the frequency components of torque ripple and current harmonics that are produced due to slot numbers of the rotor and stator for a WRIM were studied. This method can be extended to also study the rotor faults through studying the current and torque frequency spectrum. In [5], an accurate model was developed for analyzing an asymmetrical WRIM based on the reference frame theory. This proposed model relied on the machine parameters. The proposed model was confirmed against finite element simulation results

Steady-state analysis of WRIMs using impedance matrix analysis technique which can be used to investigate asymmetry faults in a wound-rotor machine was discussed [14]. A model for healthy and faulty WRIM with and without inter-turn short circuit fault by a single set of equations using modified MEC was introduced. In [11], current signature analysis was used for rotor and stator inter-turn short circuit fault detection. A proposed MATLAB–SIMULINK model for the inter-turn fault diagnosis of the induction machine via the standard deviation of the wavelet coefficient of the stator current signal was introduced in [3]. A fault index was proposed in Gritli et al. [6] as a novel method for detection of rotor faults in wound-rotor induction machines. The presented method was based on the signature analysis of the space vector that is given by the product of the space vectors of voltage and current of the rotor. The proposed approach provided some advantages over the current techniques like high sensitivity for rotor fault detections and robustness specially under time varying of operating conditions. Antonino-Daviu et al. [2] introduced an integral method based on five different fault indications to detect rotor asymmetries in WRIM. The first two indications were based on detecting families of fault harmonics appearing in the FFT spectrum of the steady-state stator current, while the second two indications relied on the analysis of the start-up stator current and the fifth evidence was based on the analysis of the rotor currents space vector spectrum (when available). In [17], the influence of the induction motor parameters

on the amplitude and the duration of both the electrical and the mechanical transient at switch-on of an induction motor was analyzed. Also the detectability of the rotor asymmetries was examined by synchrosqueezed wavelet transform (SWT).

In addition to inter-turn short circuit, increasing resistance or open circuit of one or more of the rotor windings or brush-gear circuits are one of the common rotor faults of WRIM.

It was observed that the WRIM with opening one phase in rotor circuit was capable of running at another stable speed, approximately one half of its synchronous speed, with efficiency much higher than that of the balanced motor operated at the same speed with external rotor resistances [8]. This phenomenon is called Georges phenomenon. However, although the possibility of reasonably efficient half-speed operation is attractive, this method is hardly ever used in practice due to the injection of low-frequency currents into the supply, mechanical vibration and magnetic saturation which leads to excessive currents.

The stator windings of the three-phase induction motor are supplied by alternative currents having a frequency F_s. These currents will create a rotating magnetic field at the synchronous speed n_s. If the rotor is running at a speed n (mechanical rotation speed), induced current having a frequency of SF_s will be induced in the remaining rotor short-circuited single-phase windings. The induced rotor current will then create a pulsating magnetic field which can be divided into two rotating magnetic fields. The first will rotate at the synchronous speed n_s, and the second will rotate at the speed of $(1-2S)\ n_s$ with respect to stator frame. The interaction between the rotating magnetic field created by stator windings and the first rotor rotating magnetic field will result in a motoring torque, while the interaction between the stator rotating magnetic field and the second rotor rotating magnetic field will result in a pulsating torque which has zero average value. However, the second rotor rotating magnetic field will induce currents in stator windings. By acting on these induced currents, the second rotor rotating field will create a new torque. This new torque will have the tendency to move the rotor in the forward direction if the speed is lower than half-synchronous speed (i.e., $S>0.5$) and in backward direction if the speed is higher than half-synchronous speed (i.e., $S<0.5$). So the motor could operate at a stable speed near to half its synchronous speed [16]. In [9], the operation of induction motors with Georges phenomenon was studied, and an equivalent circuit was derived for the general case of unbalance in rotors windings.

Although theoretical principles have been given to induction motors with open one rotor phase, no attempts have been made on studying the motor performance and analyzing the stator and rotor currents during this fault. So in this paper, the dynamic performance of the WRIM under healthy and rotor windings asymmetry with one-open-phase fault conditions is analyzed. The simulation and hardware verification show that the ripples of speed and torque have increased, also the stator and rotor currents have increased. Analysis of the motor performance with different rotor windings connections shows that the performance of the motor under asymmetry conditions depends on the type of connection of the rotor windings and fault location. The motor performance was studied for the case of starting the motor with an open circuit in the rotor and for the case of opening one rotor phase during normal operation. The Georges phenomenon is discussed thoroughly at different cases. A special delta connection for the rotor winding

was proposed to reduce the effect of the Georges phenomenon. Furthermore, the stator and rotor currents are analyzed using FFT technique to identify the fault signatures.

The rest of this paper is organized as follows: the dynamic models of the WRIM under healthy condition and with an open circuit in the rotor circuit for four different possible connections of rotor windings are presented in Section "Wound-Rotor Induction Motor Modeling." Section "Simulation Results" presents the simulation results for different cases. In Section "Experimental Results," the experimental results are presented to verify the simulation results. Section "Discussion" gives the discussions and analysis of the obtained results. Finally, the conclusions are given in Section "Conclusions."

Wound-rotor induction motor modeling

Healthy motor model

The dynamic model of the WRIM can be built under healthy condition in the ABC frame as functions of rotor position by its voltage differential and mechanical equations as follows:

$$\begin{bmatrix} V_{\mathrm{s}} \\ V_{\mathrm{r}} \end{bmatrix} = \begin{bmatrix} Z_{\mathrm{ss}} & Z_{\mathrm{sr}} \\ Z_{\mathrm{rs}} & Z_{\mathrm{rr}} \end{bmatrix} \begin{bmatrix} I_{\mathrm{s}} \\ I_{\mathrm{r}} \end{bmatrix} \tag{1}$$

Where

$$[V_{\mathrm{s}}] = \begin{bmatrix} v_{\mathrm{as}} & v_{\mathrm{bs}} & v_{\mathrm{cs}} \end{bmatrix}^{\mathrm{T}}, \quad [V_{\mathrm{r}}] = \begin{bmatrix} 0 & 0 & 0 \end{bmatrix}^{\mathrm{T}} \tag{2}$$

$$[I_{\mathrm{s}}] = \begin{bmatrix} i_{\mathrm{as}} & i_{\mathrm{bs}} & i_{\mathrm{cs}} \end{bmatrix}^{\mathrm{T}}, \quad [I_{\mathrm{r}}] = \begin{bmatrix} i_{\mathrm{ar}} & i_{\mathrm{br}} & i_{\mathrm{cr}} \end{bmatrix}^{\mathrm{T}} \tag{3}$$

$$[Z_{\mathrm{ss}}] = \begin{bmatrix} R_{\mathrm{s}} + L_{\mathrm{s}}p & -0.5L_{\mathrm{o}}p & -0.5L_{\mathrm{o}}p \\ -0.5L_{\mathrm{o}}p & R_{\mathrm{s}} + L_{\mathrm{s}}p & -0.5L_{\mathrm{o}}p \\ -0.5L_{\mathrm{o}}p & -0.5L_{\mathrm{o}}p & R_{\mathrm{s}} + L_{\mathrm{s}}p \end{bmatrix} \tag{4}$$

$$[Z_{\mathrm{rr}}] = \begin{bmatrix} R_{\mathrm{r}} + L_{\mathrm{r}}p & -0.5L_{\mathrm{o}}p & -0.5L_{\mathrm{o}}p \\ -0.5L_{\mathrm{o}}p & R_{\mathrm{r}} + L_{\mathrm{r}}p & -0.5L_{\mathrm{o}}p \\ -0.5L_{\mathrm{o}}p & -0.5L_{\mathrm{o}}p & R_{\mathrm{r}} + L_{\mathrm{r}}p \end{bmatrix} \tag{5}$$

$$[Z_{\mathrm{sr}}] = L_{\mathrm{o}}p \begin{bmatrix} \cos(\theta_{\mathrm{r}}) & \cos(\theta_{\mathrm{r}} - 2\pi/3) & \cos(\theta_{\mathrm{r}} + 2\pi/3) \\ \cos(\theta_{\mathrm{r}} + 2\pi/3) & \cos(\theta_{\mathrm{r}}) & \cos(\theta_{\mathrm{r}} - 2\pi/3) \\ \cos(\theta_{\mathrm{r}} - 2\pi/3) & \cos(\theta_{\mathrm{r}} + 2\pi/3) & \cos(\theta_{\mathrm{r}}) \end{bmatrix} \tag{6}$$

$$[Z_{\mathrm{rs}}] = [Z_{\mathrm{sr}}]^{\mathrm{T}} \tag{7}$$

$$L_{\mathrm{s}} = L_{\mathrm{ls}} + L_{\mathrm{o}}, \quad L_{\mathrm{r}} = L_{\mathrm{lr}} + L_{\mathrm{o}} \tag{8}$$

$$T_{\mathrm{em}} = \frac{P}{2} \begin{bmatrix} I_{\mathrm{s}} \\ I_{\mathrm{r}} \end{bmatrix}^{\mathrm{T}} \frac{\mathrm{d}L}{\mathrm{d}\theta_{\mathrm{r}}} \begin{bmatrix} I_{\mathrm{s}} \\ I_{\mathrm{r}} \end{bmatrix} \tag{9}$$

$$T_{\mathrm{em}} - T_{\mathrm{load}} = J\frac{\mathrm{d}\omega_m}{\mathrm{d}t} + B\omega + T_{\mathrm{f}} \tag{10}$$

$$p\theta_{\mathrm{r}} = \omega_{\mathrm{r}} = P\omega_m \tag{11}$$

$$p = \frac{\mathrm{d}}{\mathrm{d}t} \tag{12}$$

Open-phase motor models

The dynamic model of the WRIM is modified to represent the open rotor phase condition. The stator windings of the studied motor are connected as star connection, while the rotor windings could be star or delta connection. The rotor windings could be connected in different four connections, which are isolated neutral star connection, standard delta connection with internal open circuit rotor phase, standard delta connection with external open circuit rotor phase and delta connection with reversed one phase and external open circuit. These connections are shown in Fig. 1.

Isolated neutral star connection

When one rotor phase is open-circuited in case of isolated neutral star connection, the other two phases become connected in series as shown in Fig. 1a. So the voltage differential equations can be rewritten as in healthy case with the following changes:

$$[V_{\mathrm{r}}] = [0] \tag{13}$$

$$[I_{\mathrm{r}}] = [i_{\mathrm{r}}], \quad i_{\mathrm{ar}} = -i_{\mathrm{br}} = i_{\mathrm{r}} \tag{14}$$

$$[Z_{\mathrm{rr}}] = [2R_{\mathrm{r}} + (2L_{\mathrm{lr}} + 3L_{\mathrm{o}})p] \tag{15}$$

$$[Z_{\mathrm{sr}}] = L_{\mathrm{o}}p\begin{bmatrix} \cos(\theta_{\mathrm{r}}) - \cos(\theta_{\mathrm{r}} - 2\pi/3) \\ \cos(\theta_{\mathrm{r}} + 2\pi/3) - \cos(\theta_{\mathrm{r}}) \\ \cos(\theta_{\mathrm{r}} - 2\pi/3) - \cos(\theta_{\mathrm{r}} + 2\pi/3) \end{bmatrix} \tag{16}$$

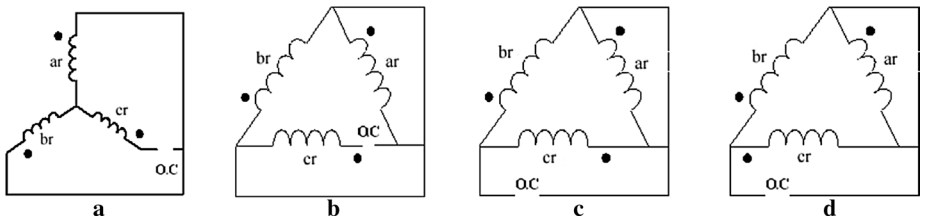

Fig. 1 Different connections of rotor windings: **a** isolated neutral star connection, **b** standard delta connection with internal open circuit, **c** standard delta connection with external open circuit and **d** delta connection with reversed one phase and external open circuit

Standard delta connection with internal open circuit rotor phase

For standard delta with internal open circuit, when one rotor phase is internally open-circuited, each phase of the other two phases will be short-circuited upon itself as shown in Fig. 1b, the voltage differential equations can be rewritten with the following changes:

$$[V_{\mathrm{r}}] = \begin{bmatrix} 0 & 0 \end{bmatrix}^{\mathrm{T}} \tag{17}$$

$$[I_{\mathrm{r}}] = \begin{bmatrix} i_{\mathrm{ar}} & i_{\mathrm{br}} \end{bmatrix}^{\mathrm{T}} \tag{18}$$

$$[Z_{\mathrm{rr}}] = \begin{bmatrix} R_{\mathrm{r}} + L_{\mathrm{r}}p & -0.5L_{\mathrm{o}}p \\ -0.5L_{\mathrm{o}}p & R_{\mathrm{r}} + L_{\mathrm{r}}p \end{bmatrix} \tag{19}$$

$$[Z_{\mathrm{sr}}] = L_{\mathrm{o}}p \begin{bmatrix} \cos(\theta_{\mathrm{r}}) & \cos(\theta_{\mathrm{r}} - 2\pi/3) \\ \cos(\theta_{\mathrm{r}} + 2\pi/3) & \cos(\theta_{\mathrm{r}}) \\ \cos(\theta_{\mathrm{r}} - 2\pi/3) & \cos(\theta_{\mathrm{r}} + 2\pi/3) \end{bmatrix} \tag{20}$$

Standard delta connection with external open circuit phase

In case of standard delta connection with external open circuit, when one rotor phase is externally open-circuited, two of rotor phases are connected in series and the combination of them is connected in parallel with the third phase, the voltage differential equations of the this configuration can be rewritten as in healthy case with the following changes:

$$[V_{\mathrm{r}}] = \begin{bmatrix} 0 & 0 \end{bmatrix}^{\mathrm{T}} \tag{21}$$

$$[I_{\mathrm{r}}] = \begin{bmatrix} i_{\mathrm{ar}} & i_{\mathrm{br}} \end{bmatrix}^{\mathrm{T}} \tag{22}$$

$$[Z_{\mathrm{rr}}] = \begin{bmatrix} R_{\mathrm{r}} + L_{\mathrm{r}}p & -L_{\mathrm{o}}p \\ -L_{\mathrm{o}}p & 2R_{\mathrm{r}} + (2L_{\mathrm{r}} + L_{\mathrm{o}})p \end{bmatrix} \tag{23}$$

$$[Z_{\mathrm{sr}}] = L_{\mathrm{o}}p \begin{bmatrix} \cos(\theta_{\mathrm{r}}) & \cos(\theta_{\mathrm{r}} + 2\pi/3) + \cos(\theta_{\mathrm{r}} - 2\pi/3) \\ \cos(\theta_{\mathrm{r}} + 2\pi/3) & \cos(\theta_{\mathrm{r}}) + \cos(\theta_{\mathrm{r}} + 2\pi/3) \\ \cos(\theta_{\mathrm{r}} - 2\pi/3) & \cos(\theta_{\mathrm{r}} - 2\pi/3) + \cos(\theta_{\mathrm{r}}) \end{bmatrix} \tag{24}$$

Delta connection with reversed one phase and external open circuit rotor phase

For delta connection with reversed one, when one rotor phase is externally open-circuited, two of rotor phases are connected in series and the combination of them is connected in parallel with the third phase, the voltage differential equations of the this configuration can be rewritten as in healthy case with the following changes:

$$[V_{\mathrm{r}}] = \begin{bmatrix} 0 & 0 \end{bmatrix}^{\mathrm{T}} \tag{25}$$

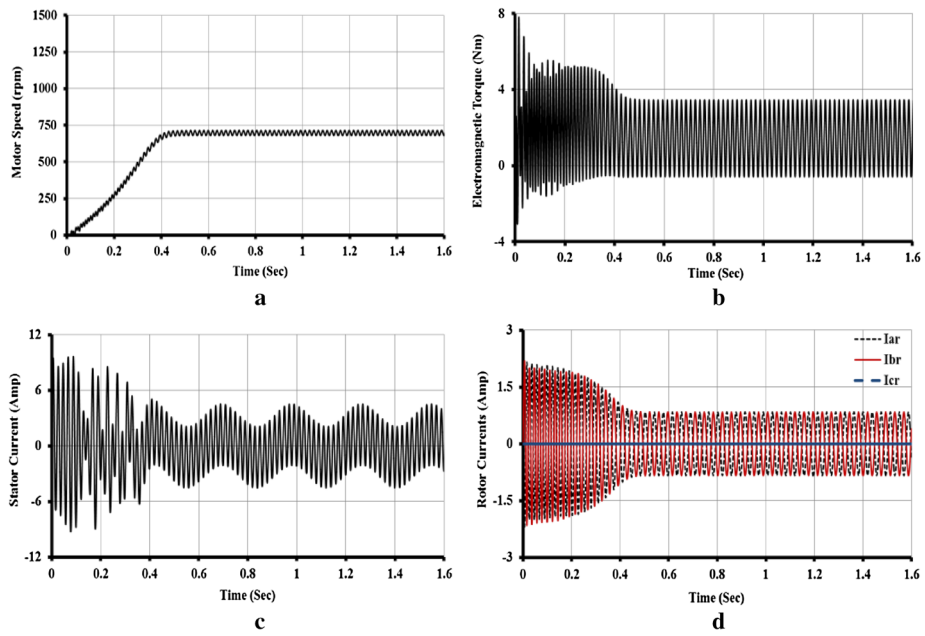

Fig. 2 Motor performance for isolated neutral star connection, **a** motor speed, **b** electromagnetic torque, **c** stator phase current and **d** rotor currents

$$[I_{\mathrm{r}}] = \begin{bmatrix} i_{\mathrm{ar}} & i_{\mathrm{br}} \end{bmatrix}^{\mathrm{T}} \tag{26}$$

$$[Z_{\mathrm{rr}}] = \begin{bmatrix} R_{\mathrm{r}} + L_{\mathrm{r}}p & 0 \\ 0 & 2R_{\mathrm{r}} + (2L_{\mathrm{r}} + 3L_{\mathrm{o}})p \end{bmatrix} \tag{27}$$

$$[Z_{\mathrm{sr}}] = L_{\mathrm{o}}p \begin{bmatrix} \cos(\theta_{\mathrm{r}}) & \cos(\theta_{\mathrm{r}} + 2\pi/3) - \cos(\theta_{\mathrm{r}} - 2\pi/3) \\ \cos(\theta_{\mathrm{r}} + 2\pi/3) & \cos(\theta_{\mathrm{r}}) - \cos(\theta_{\mathrm{r}} + 2\pi/3) \\ \cos(\theta_{\mathrm{r}} - 2\pi/3) & \cos(\theta_{\mathrm{r}} - 2\pi/3) - \cos(\theta_{\mathrm{r}}) \end{bmatrix} \tag{28}$$

Simulation results

The experimental and simulation results have been carried out on a 4-pole, 175 W, 110 V, 1.9 A, 1370 rpm, 50-HZ three-phase wound-rotor induction motor. The fault is modeled by starting the motor with opening one phase of rotor circuit. The motor is loaded with its full load torque, and the four possible connections of the rotor windings are considered. Due to the asymmetry that occurs in rotor circuit, the rotor magnetic field in the air gap of the motor is not a pure rotating field as in the healthy case so it affects the performance of the motor as illustrated in the following figures for the different cases of rotor windings connections.

The motor speed, electromagnetic torque, stator phase current and the rotor currents are presented in Fig. 2 for the case of isolated neutral star connection. As shown in Fig. 2a, the motor operates at a speed close to half of its synchronous speed (697 rpm) and the speed has noticeable ripples at steady state. Furthermore, the steady-state torque is a pulsating torque as shown in Fig. 2b due to the backward component of the rotor

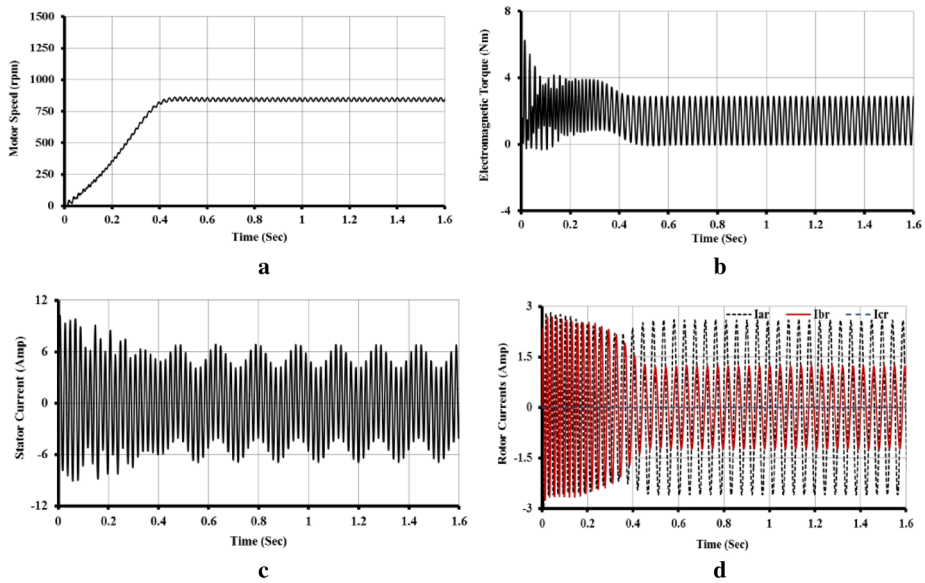

Fig. 3 Motor performance for standard delta with internal open circuit rotor phase windings connections, **a** motor speed, **b** electromagnetic torque, **c** stator phase current and **d** rotor currents

MMF. Figure 2c shows the phase current of the stator. It is clear that the stator current is oscillatory and reaches with harmonics. Additionally, the currents of the two phases of rotor are equal in magnitude, but they are shifted by 180 electric degrees as shown in Fig. 2d.

Figure 3 shows the motor speed, electromagnetic torque, stator phase current and rotor currents in the case of standard delta connection with internal open circuit rotor phase. Similarly, the motor operates at a speed near to half of its synchronous speed (840 rpm) with noticeable ripples at steady state as shown in Fig. 3a. Also the steady-state torque is a pulsating torque as shown in Fig. 3b. In this case, the oscillatory stator current is shown in Fig. 3c. Additionally, the currents of the rotor are not equal in magnitude as shown in Fig. 3d.

The motor speed, electromagnetic torque, stator phase current and the rotor currents are presented in Fig. 4 for the case of standard delta connection with external open circuit. As shown in Fig. 4a, the motor operates at a speed near to half of its synchronous speed (697 rpm) and the speed has noticeable ripples at steady state. Furthermore, the steady-state torque is a pulsating torque as shown in Fig. 4b due to the strong backward component of the rotor MMF. Figure 4c shows the phase current of the stator. It is clear that the stator current is oscillatory and reaches with harmonics. Additionally, the current of the two series connected phases of rotor is equal to one half of the rms value of the third phase, but they are shifted by 180 electric degrees as shown in Fig. 4d.

Figure 5 shows the motor performance for the case of delta connection with reversed one phase and external open circuit. The motor operates at a speed of 1350 rpm which is less lightly than its full load speed and with minimum ripples as shown in Fig. 5a. The motor torque has noticeable ripples at steady state as shown in Fig. 5b. The stator current has less oscillation as shown in Fig. 5c. Finally, the currents of the phase "br" and

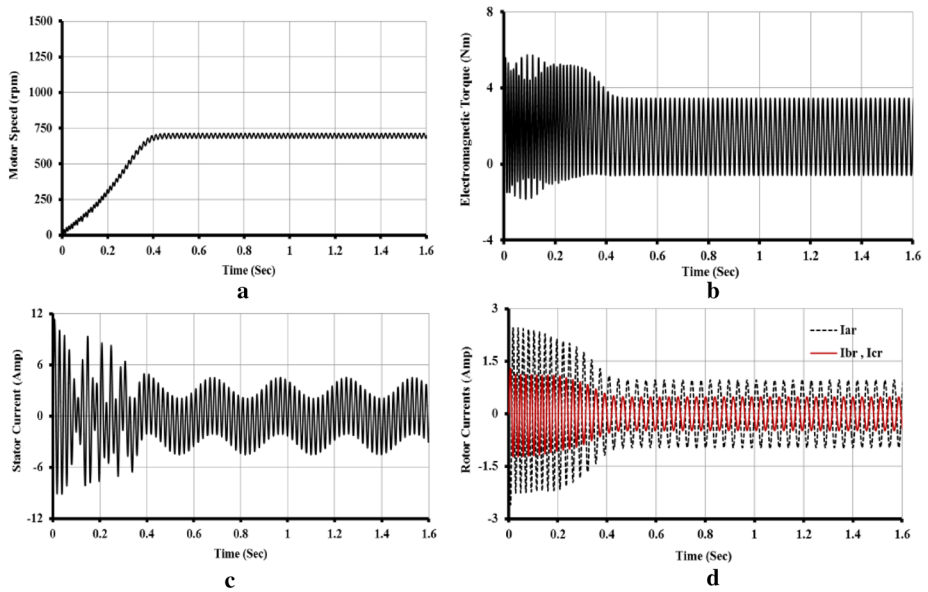

Fig. 4 Motor performance for standard delta with external open circuit rotor windings connection, **a** motor speed, **b** electromagnetic torque, **c** stator phase current and **d** rotor currents

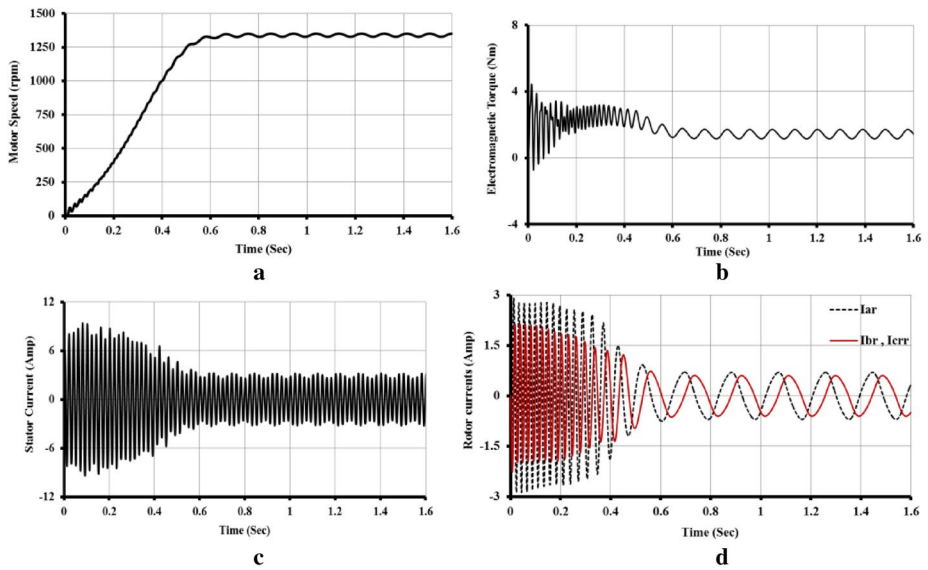

Fig. 5 Motor performance for delta with reversed one phase and external open circuit rotor windings connection, **a** motor speed, **b** electromagnetic torque, **c** stator phase current and **d** rotor currents

phase "cr" of the rotor are the same since they are connected in series, while the current of phase "ar" is shifted by 90 electric degrees from the other two phases as shown in Fig. 5d.

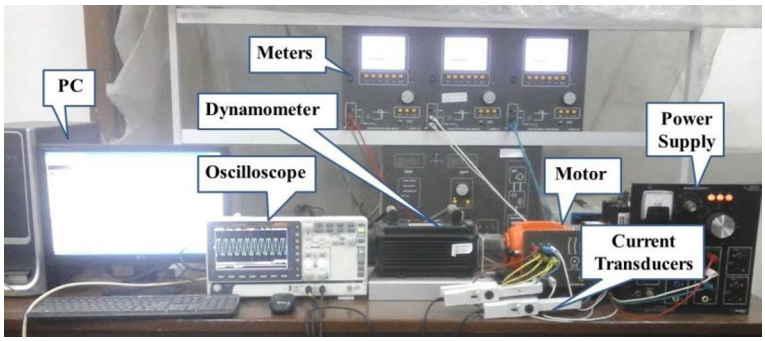

Fig. 6 The experimental setup at the laboratory

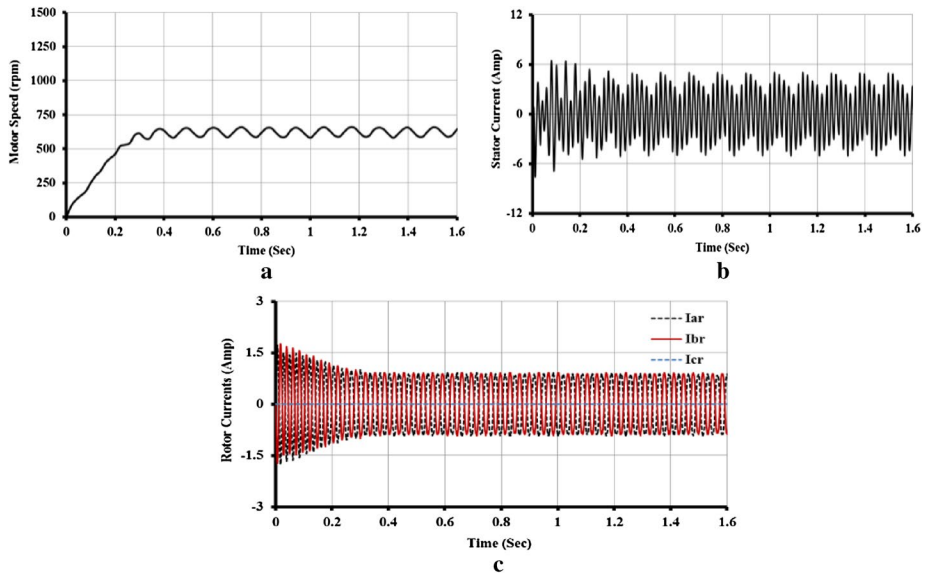

Fig. 7 Experimental results for isolated neutral star connection, **a** motor speed, **b** stator phase current and **c** rotor currents

Experimental results

Several experiments were carried out to confirm the simulation results for the case of starting the WRIM with opening one rotor phase with the four possible rotor connections considered. The image of the experimental setup at the laboratory is presented in Fig. 6. The motor speed, stator and rotor currents have been collected and saved via a digital oscilloscope, and then, the saved data have been plotted using a software package. The motor is loaded by a dynamometer and fed from a constant-voltage constant-frequency three-phase supply as shown in Fig. 6. The data acquisition unit consists of digital oscilloscope, current transducers and personal computer as shown in Fig. 6.

Figure 7 shows the motor performance in the case of isolated neutral star connected rotor windings. The motor operates at speed near to half of its synchronous speed, and the ripples of speed at steady state have increased as shown in Fig. 7a. It is clear that the stator current is oscillatory and with harmonics content as shown in Fig. 7b.

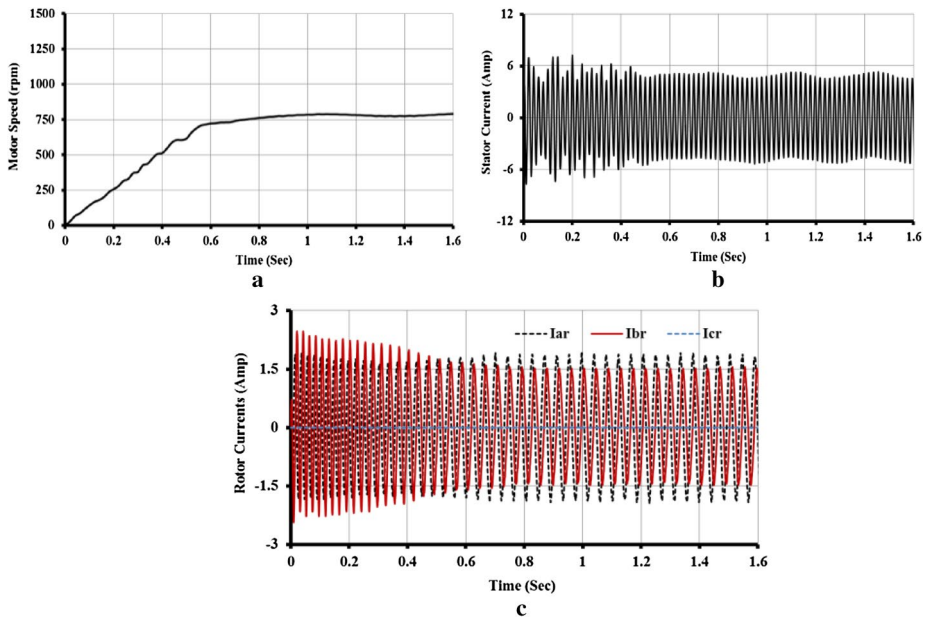

Fig. 8 Experimental results for standard delta connection with internal open circuit rotor phase, **a** motor speed, **b** stator phase current and **c** rotor currents

Additionally, the rms value of rotor currents in this faulty case has increased and the currents of the two phases of rotor are equal in magnitude, but they are shifted by 180 electric degrees as shown in Fig. 7c. Figure 8 shows the motor speed, stator phase current and the rotor currents for the case of rotor windings with standard delta connection and internal open circuit rotor phase. The motor operates at a speed near to half of its synchronous speed with noticeable ripples at steady state as shown in Fig. 8a. In this case, the stator current is oscillatory as shown in Fig. 8b. Additionally, the currents of the two phases of rotor are not equal in magnitude, but they are shifted by 120 electric as shown in Fig. 8c.The motor performance in the case of standard delta connection with external open circuit is shown in Fig. 9. The motor operates at speed near to half of its synchronous speed, and the ripples of speed at steady state have increased as shown in Fig. 9a. Figure 9b shows the stator current; it is clear that the stator current is oscillatory and with harmonics content. Additionally, the current of the two series connected phases of the rotor is equal to one half of the rms value of the third phase, but they are shifted by 180 electric degrees as shown in Fig. 9c. Figure 10 shows the motor performance for the case of delta connection with reversed one phase and external open circuit. The motor operates at a speed slightly less than the full load speed with ripples and a starting time higher than that of the healthy case as shown in Fig. 10a. The stator current has fewer oscillations compared to star connection as shown in Fig. 10b. Finally, the currents of the (phase-br) and (phase-cr) of the rotor are the same since they are connected in series. The current of (phase-ar) is different and is shifted by 90 electric degrees from the other two phases as shown in Fig. 10c. Table 1 gives a comparison between the simulation and experimental results. Good agreement has been achieved between the simulation and experimental results.

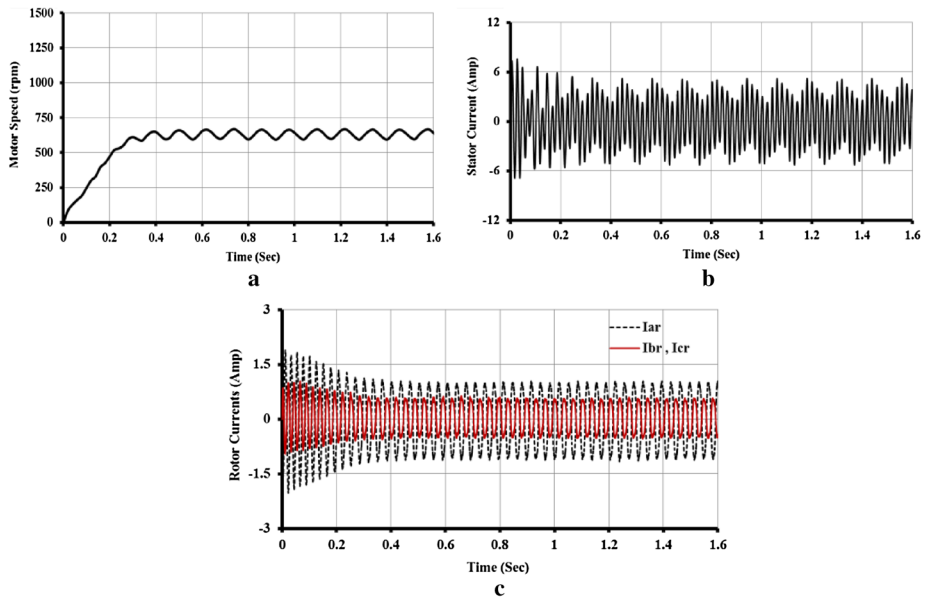

Fig. 9 Experimental results for standard delta connection with external open circuit, **a** motor speed, **b** stator phase current and **c** rotor currents

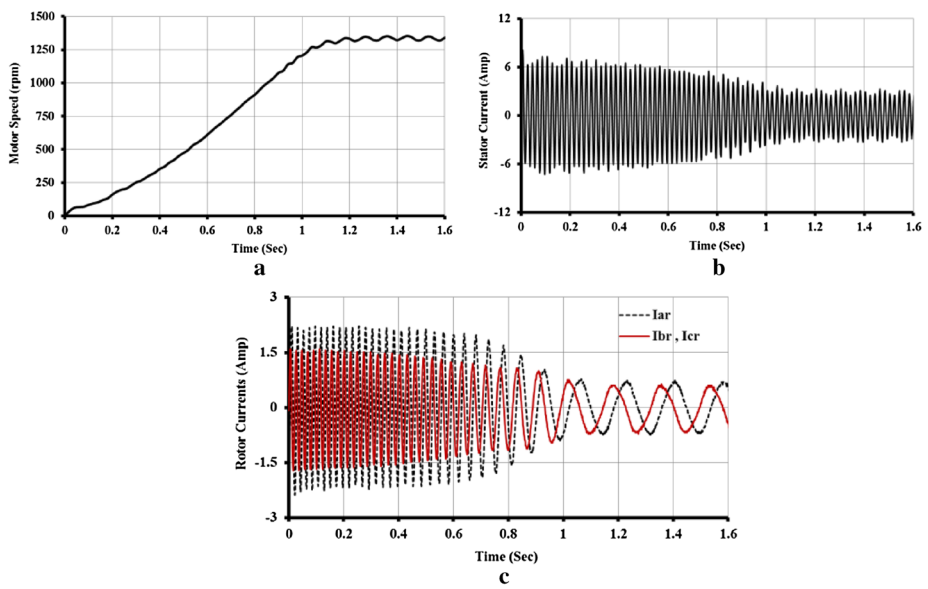

Fig. 10 Experimental results for delta with reversed one phase and external open circuit rotor windings connection, **a** motor speed, **b** stator phase current and **c** rotor currents

The torque speed curves under healthy and faulty conditions for different connections of rotor windings are measured and plotted experimentally as shown in Fig. 11. Figure 11a shows the torque speed curve for isolated neutral star connection. It can be noticed that the motor operates either close to half of its synchronous speed or at a speed slightly less than the full load speed according to the value of its loading and the

Table 1 Summarized simulation and experimental results

Case		n (rpm)	Speed ripples (%)	Torque ripples (%)	I_{as} (A)	I_{ar} (A)	I_{br} (A)	I_{cr} (A)
Healthy case	Simulation	1375	0	0	2.07	0.41	0.41	0.41
	Experimental	1370	0.3		1.9	0.4	0.4	0.4
Isolated neutral star	Simulation	697	4.8	280	2.62	0.6	0.6	0
	Experimental	620	8.5		2.8	0.68	0.68	0
Standard delta connection with internal open circuit	Simulation	840	2.3	150	4.1	1.85	0.89	0
	Experimental	780	2.6		3.4	1.3	0.996	0
Standard delta connection with external open circuit	Simulation	697	4.9	275	2.63	0.67	0.34	0.34
	Experimental	622	8.5		2.82	0.74	0.37	0.37
Delta connection with reversed one phase and external open circuit	Simulation	1350	1.8	25	2.06	0.5	0.435	0.435
	Experimental	1335	2.2		2.0	0.49	0.42	0.42

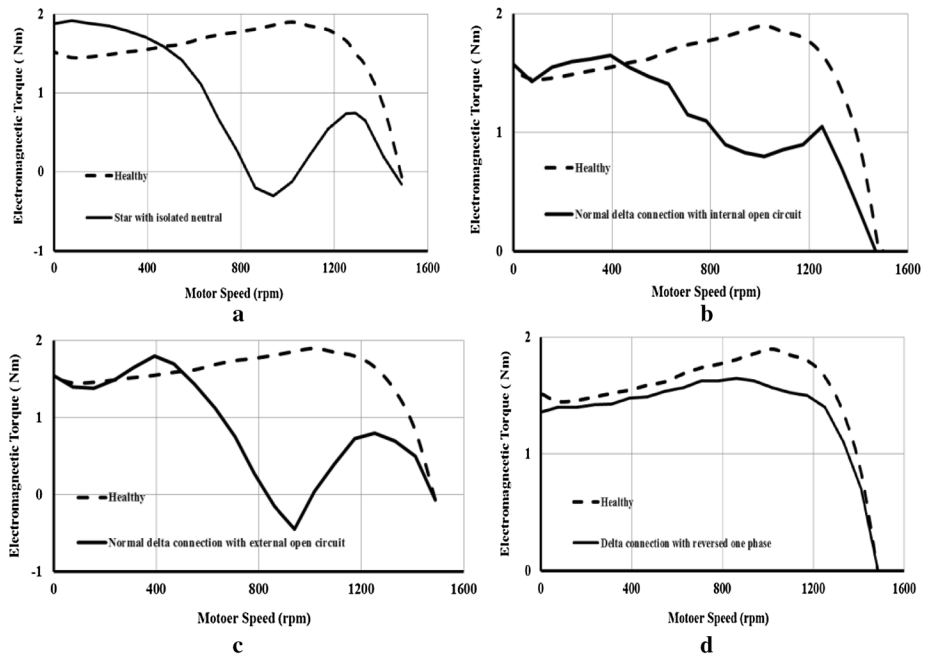

Fig. 11 Experimental results for the torque speed characteristics for, **a** isolated neutral star connection, **b** standard delta with internal open circuit, **c** standard delta with external open circuit and **d** delta connection with reversed one phase

instant of the occurrence of fault; the Georges phenomenon is very clear in this case. The torque speed curve for standard delta connection with internal open circuit rotor phase is shown in Fig. 11b. It can be observed that the motor operates either close to half of its synchronous speed or at a speed slightly less than the full load speed according to the value of the load torque and the instant of fault occurrence. Figure 11c shows the torque speed curve for standard delta connection with external open circuit rotor phase. It can be observed that the motor operates close to half of its synchronous speed at any value of load torque if the motor is stared with opening one phase of rotor circuit. Also

Table 2 Torque limits of the occurrence of Georges phenomenon

Rotor connection	Instant of fault	The value of load torque	Gorges phenomenon
Isolated neutral star	Starting with opening one phase	Up to full load	Occurs
	Opening one phase during normal operation	< 67% of its full load	Does not occur
Standard delta connection with external open phase	Starting with opening one phase	Up to full load	Occurs
	Opening one phase during normal operation	< 67% of its full load	Does not occur
Standard delta connection with internal open phase	Starting with opening one phase	< 87.5% of its full load	Does not occur
	Opening one phase during normal operation	Up to full load	Does not occur
Delta connection with reversed one phase and external open circuit	Starting with opening one phase	Up to full load	Does not occur
	Opening one phase during normal operation	Up to full load	Does not occur

the Georges phenomenon is very clear for this case. Figure 11d shows the torque speed curve for delta connection with reversed one phase and external open circuit rotor phase case and healthy condition. It can be noted that the two curves are very similarly but with small difference in the values of starting and maximum torques. So for this connection, the motor operates at a speed slightly less than the healthy speed at any value of its loading regardless of the instant of opening one phase of its rotor phases. Table 2 shows the limit values of load torque at which the Georges phenomenon occurs for different rotor windings connections.

Furthermore, the experimental stator and rotor currents are analyzed using fast Fourier transformation (FFT) technique. Figure 12 shows the current spectrum in the case of isolated neutral star connection rotor windings. In this case, the motor operated at a speed of 620 rpm, and hence, the motor slip is equal to 0.586. Here, the sidebands harmonics of fundamental harmonic $(1 \pm 2S)Fs$ are clearly observed at 8.5 Hz and 108.5 Hz in the stator phase current spectrum as shown in Fig. 12a. Also it can be clearly observed that there is additional one sideband harmonic at $(1-4S)F_s$ with frequency of 66.5 Hz. In addition, the presence of third harmonic $3SF_s$ is observed in rotor currents with frequency of 87.81 Hz as shown in Fig. 12b, c.

Figure 13 shows the spectrums of stator current and rotor currents for standard delta connection with internal open circuit, the motor operated at a speed of 780 rpm, and hence the motor slip is equal to 0.48. The sidebands harmonics of fundamental harmonic are noticeably at 3 Hz and 97.25 Hz in the stator phase current spectrum as shown in Fig. 13a. In addition, the presence of third harmonic appears in the rotor currents with frequency of 70.75 Hz as shown in Fig. 13b, c. The current spectrums in the case of standard delta connection with external open circuit are shown in Fig. 14, the motor operated at a speed of 622 rpm, and hence the motor slip is equal to 0.585. Here, the sidebands harmonics of fundamental harmonic are clearly observed at 8.46 Hz and 109.2 Hz in stator current spectrum as shown in Fig. 14a. It can be clearly observed that there is additional one sideband harmonic at frequency of 66.7 Hz. Also the presence of third harmonic is observed in rotor currents with frequency of 86.7 Hz as shown

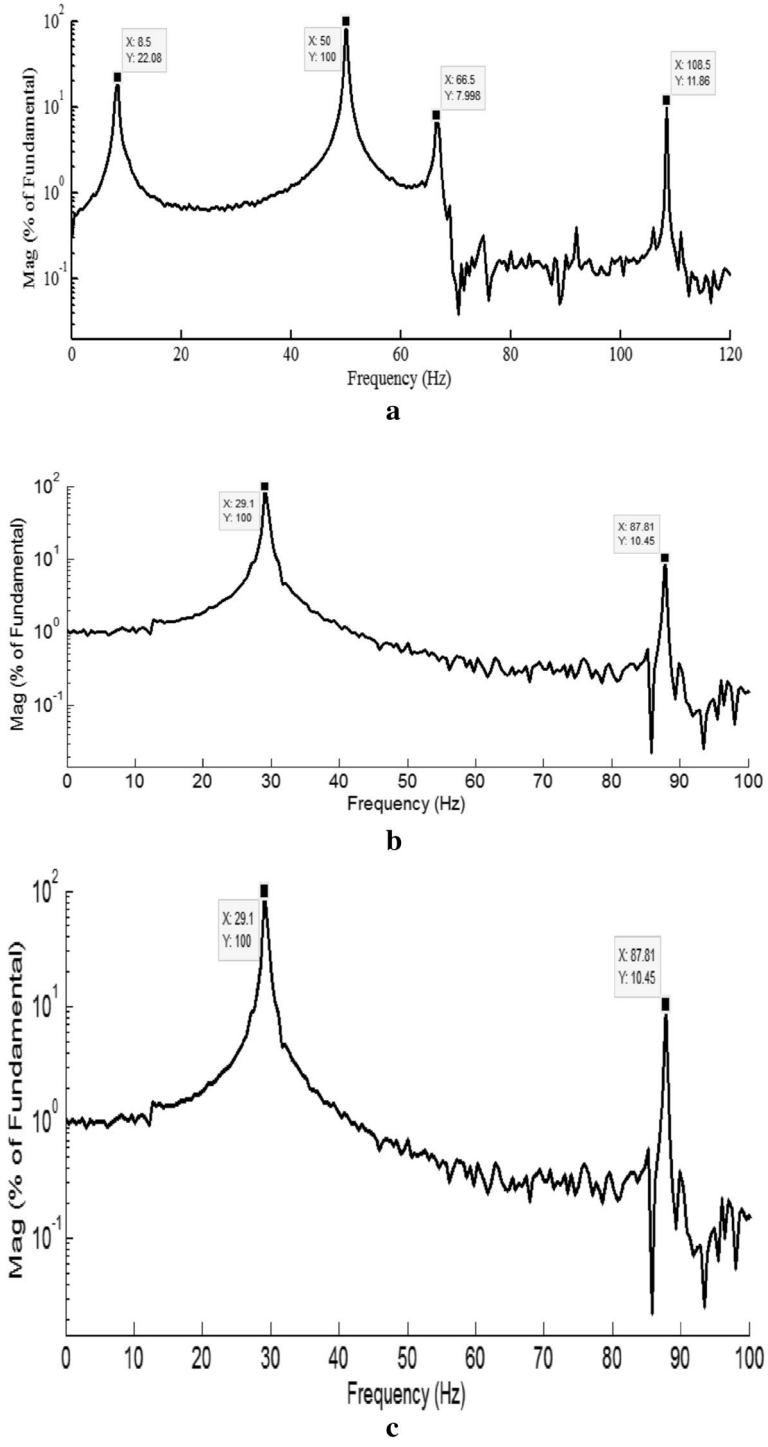

Fig. 12 Current spectrums for isolated neutral star connection, **a** stator phase current, **b** rotor (phase-ar) current and **c** rotor (phase-br) current

in Fig. 14b, c. Figure 15 shows the current spectrum for the case of delta connection with reversed one phase and external open circuit, the motor operated at a speed of 1335 rpm, and hence the motor slip is equal to 0.11. Here, the sidebands harmonics

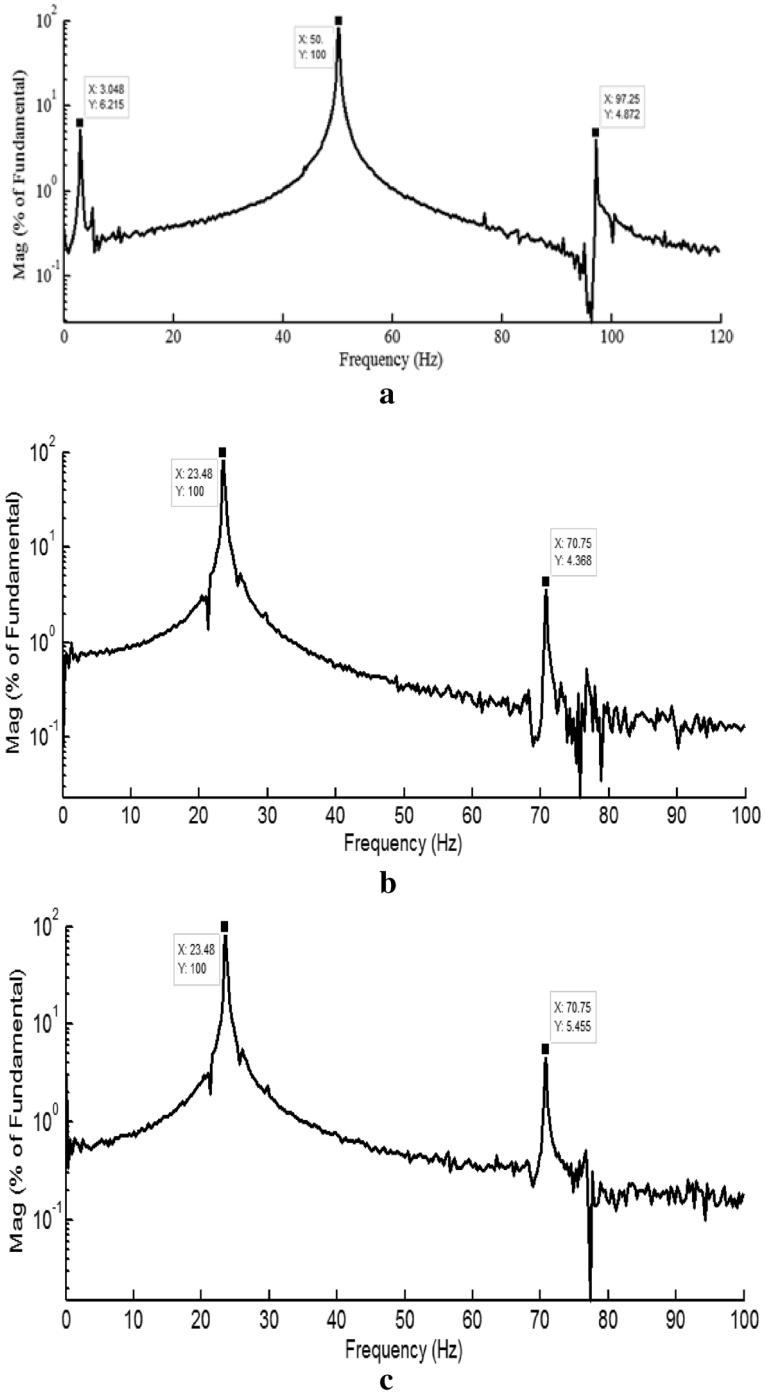

Fig. 13 Current spectrums for standard delta connection with internal open circuit, **a** stator phase current, **b** rotor (phase-ar) current and **c** rotor (phase-br) current

of fundamental harmonic are clearly observed at 38.67 Hz and 61.33 Hz in the stator phase current spectrum. There is additional one sideband harmonic at a frequency of 27.33 Hz as shown in Fig. 15a. The third harmonic is observed in the rotor currents with frequency of 16.86 Hz as shown in Fig. 15b, c.

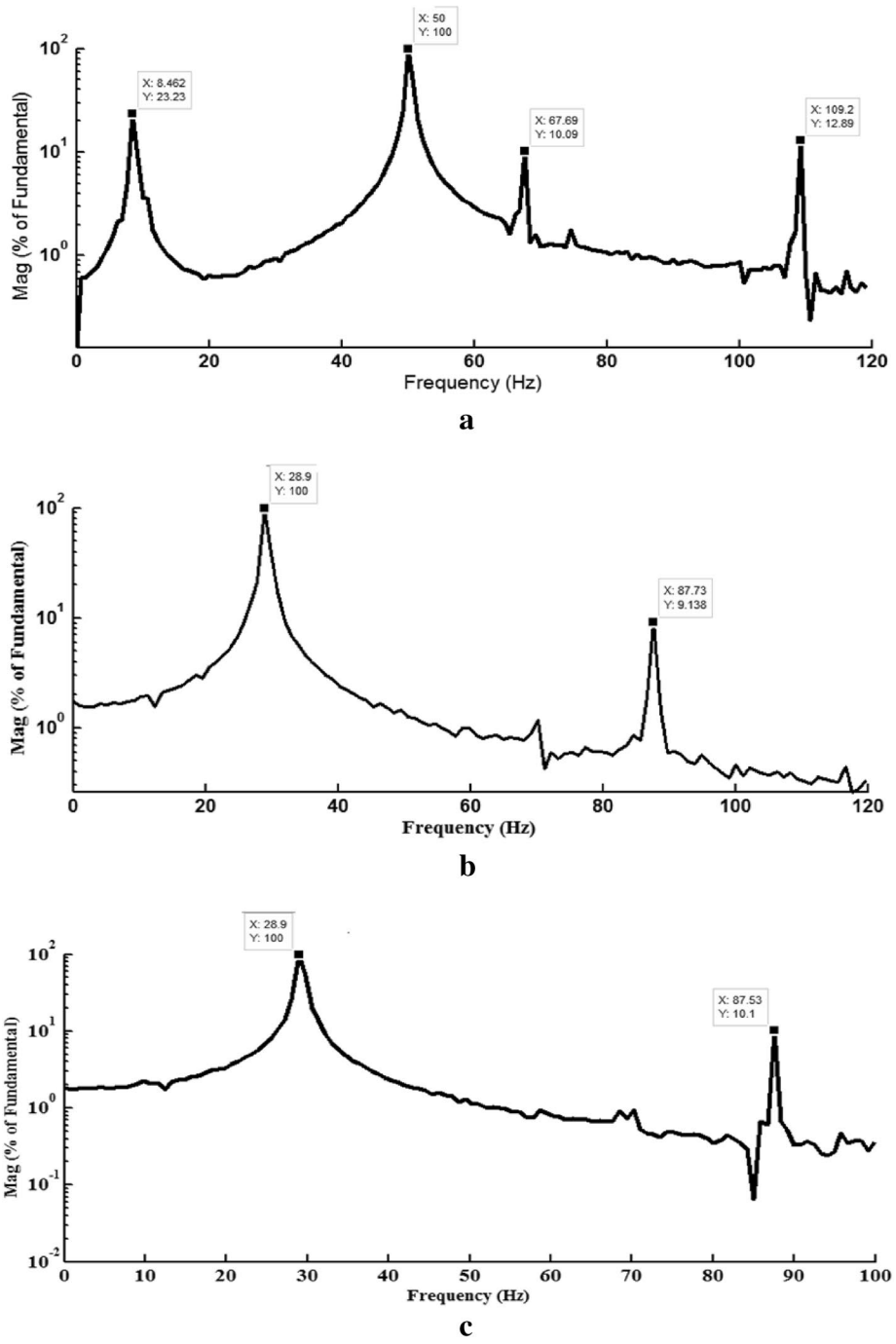

Fig. 14 Current spectrums for standard delta with external open circuit, **a** stator phase current, **b** rotor (phase-ar) current and **c** rotor (phase-br) current

Discussion

From the simulation and experimental results, the following relevant points can be deduced:

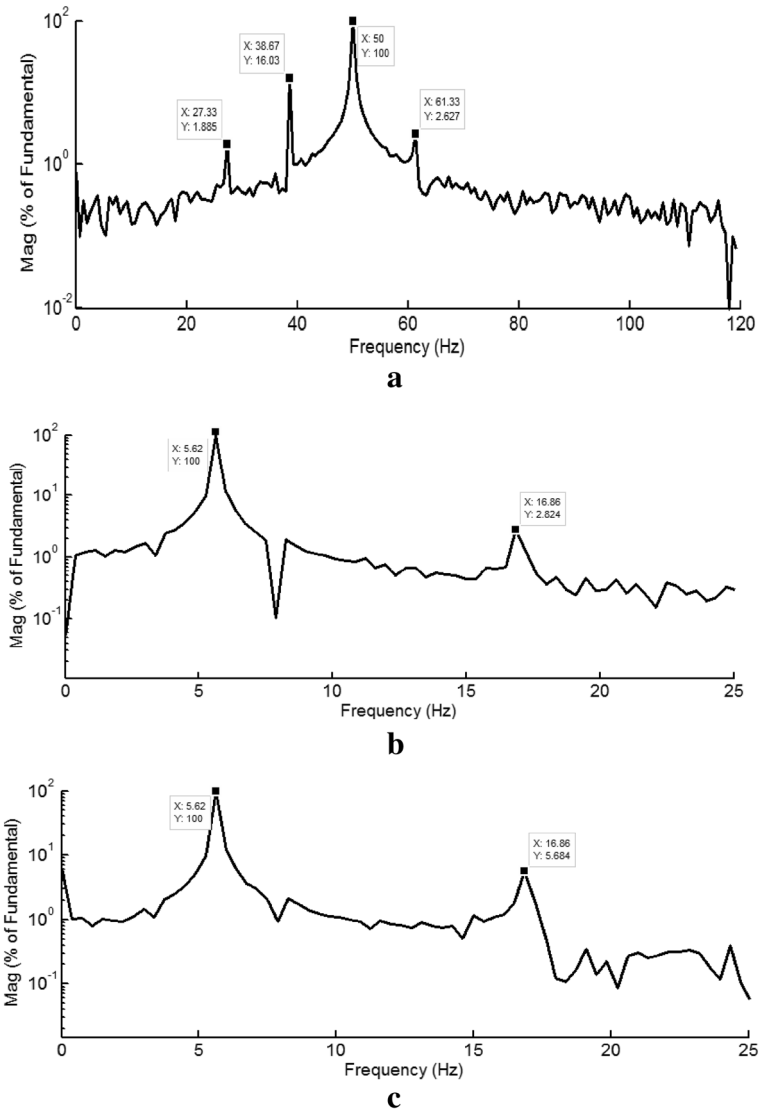

Fig. 15 Current spectrum for delta connection with reversed one phase and external open circuit, a stator phase current, **b** rotor (phase-ar) current and **c** rotor (phase-br) current

- The performance of WRIM under the condition of opening of one phase of rotor circuit depends on the connection of rotor windings. While the isolated neutral star rotor windings and standard delta connections have the worst performance, the rotor delta connected windings with reversed one phase and external open circuit has an acceptable performance.
- Opening of one phase of rotor circuit causes oscillatory and high stator currents.
- The rotor MMFs of the isolated neutral star rotor windings and standard delta with external open circuit have strong backward component, which affects the shape of the torque speed characteristic of the motor resulting in Georges phenomenon.
- The motor torque is a pulsating torque due to the backward component of the rotor MMF.

- The rotor asymmetry results in unbalanced rotor currents combined with high values for all connections especially for star connection and normal delta connection.
- For delta connected rotor windings with reversed one phase and external open circuit, the motor operates at a speed slightly less than its full load speed at any value of its loading either in case of staring the motor with opening one phase of rotor circuit or opening one phase of rotor circuit during normal running (i.e., preventing Georges phenomenon).
- In case of isolated neutral star and standard delta connection with external open circuit, the motor operates at a speed close to half of its synchronous speed in case of staring the motor with opening one phase of rotor circuit at any value of load torque. But it operates at a speed slightly less than its full load speed in case of opening one phase of rotor circuit during normal running if the load torque < 67% of its full load torque, and at speed near to half of its synchronous speed if the load torque is > 67% of its full load.
- For standard delta with internal open circuit, the motor operates at a speed slightly less than its full load speed in case of opening one phase of rotor circuit during normal running at any value of load torque. Also it operates at a speed slightly less than its full load speed in case of staring the motor with opening one phase of rotor circuit if the load torque < 87.5% of its full load torque, and at speed near to half of its synchronous speed if the load torque is > 87.5% of its full load.
- The proposed delta connection with reversed one phase prevents Georges phenomenon by 67% of possible fault cases such that if the externally open circuit is occurred at any terminal of the reversed phase.
- The rotor delta connected windings with reversed one phase and external open circuit insures the operation at a speed near to the full load speed of the motor so the motor will have good efficiency and power factor.
- The given percentage values are specified to the motor under test.

Furthermore, the FFT of the motor currents showed the following:

- As a result of connecting the symmetrical stator winding to the supply voltage, a pure rotating magnetic field at frequency F_s is produced in the motor air gap. Because of rotor asymmetry windings, the rotor currents cause two counter rotating magnetic fields at frequencies $\pm SF_s$.
- The field component of $+SF_s$ interacts with stator magnetic field to produce the steady-state torque, while the other component of $-SF_s$ will induce EMFs in stator windings with frequency $(1-2S)F_s$ and hence a current in stator windings at frequency $(1-2S)F_s$.
- The stator current component with $(1-2S)F_s$ leads to oscillations in the electromagnetic torque and motor speed at frequency $2SF_s$.
- The motor speed oscillations produced a new component of current in stator winding at frequency of $(1+2S)F_s$
- The stator current at $(1+2S)F_s$ produces a rotor EMFs at frequency $3SF_s$ and a new reaction current in the stator winding at frequency $(1-4S)F_s$, and so on.

- As a result of this interaction process, the stator current spectrum has a series of harmonic sidebands at the following frequencies:

$$F_{\mathrm{h}} = (1 \pm kS)F_{\mathrm{s}} \quad \text{where } k = 1, 2, 3, \ldots.$$

  where F_{h} are frequency components related to rotor winding asymmetry fault.
- Also the harmonic sidebands of the rotor current spectrum are given by $\pm kSF_{\mathrm{s}}$ where $k = 1, 3, 5, \ldots$.

Conclusions

This paper presents a dynamic model in the ABC frame to investigate Georges phenomenon and to analyze the performance of WRIM in case of opening one phase of rotor circuit. Four possible connections for rotor windings are considered; isolated neutral star connection, standard delta connection with internal open circuit rotor phase, standard delta connection with external open circuit rotor phase and a proposed delta connection with reversed one phase and external open circuit. Motor speed, electromagnetic torque, stator and rotor currents have been investigated for all cases. The experimental results give good agreement with the simulation results in all possible connections. The torques speed characteristics of the different connections were studied, and the George's phenomenon was thoroughly studied. The paper shows that rotor asymmetry causes oscillatory and high stator currents, also results in unbalanced rotor currents combined with high values for all connections especially for star connection and normal delta connection. The frequency spectrums for the stator and rotor currents were examined to identify the fault signatures which are stator current harmonic sidebands at $(1 \pm kS)$ F_{s} frequencies and rotor current harmonic sidebands at $\pm kSF_{\mathrm{s}}$. It is proven that the occurrence of Georges phenomenon depends upon the connection of the rotor windings, the value of the motor loading and the instant of the occurrence of the fault. The paper shows that the isolated neutral star rotor windings and standard delta connections have the worst performance. It is also proven that the proposed rotor delta connected windings with reversed one phase and external open circuit avoid Georges phenomenon in two-thirds of possible fault cases and insure the operation with an acceptable performance.

List of symbols

V_s: stator voltage vector (V); v_{as}, v_{bs}, v_{cs}: stator phase voltages (V); V_r: rotor voltage vector referred to stator (V); I_s: stator current vector (A); i_{as}, i_{bs}, i_{cs}: stator phase currents (A); I_r: rotor current vector referred to stator (A); i_{ar}, i_{br}, i_{cr}: rotor phase currents (A); Z_{ss}: stator self-impedance matrix; Z_{rr}: rotor self-impedance matrix; Z_{sr}: stator–rotor mutual-impedance matrix; Z_{rs}: rotor–stator mutual-impedance matrix; R_s: stator resistance per phase (Ω); R_r: rotor resistance per phase referred to stator (Ω); L_s: stator self-inductance per phase (H); L_r: rotor self-inductance per phase referred to stator (H); L_o: maximum mutual inductance (H); L_{ls}: stator leakage inductance per phase (H); L_{lr}: rotor leakage inductance per phase referred to stator (H); L: inductances matrix; θ_r: rotor position in electrical (rad); T_{em}: electromechanical torque (Nm); ω_r: motor speed (electrical rad/s); ω_m: motor speed (rad/s); P: number of pair-poles; J: moment of Inertia (kg m^2); B: viscosity frication coefficient (Nm/(rad/s)); T_f: friction torque (Nm); F_s: supply frequency (Hz); S: motor per unit slip.

Abbreviations

WRIM: wound-rotor induction motor; FFT: fast Fourier transformation; MEC: magnetic equivalent circuit; DWT: discrete wavelet transform; SWT: synchrosqueezed wavelet transform.

Acknowledgements
Not applicable.

Authors' contributions
RR contributed in the design, the creation of the software used in the work and interpretation of the results of the work, performed the experimental work and drafted the final manuscript. TM contributed in the design and interpretation of the results of the work and drafted the final manuscript. HH contributed in the conception, analysis, the creation of the software used in the work and interpretation of the results of the work and also revised the final manuscript. All authors read and approved the final manuscript.

Funding
Not applicable.

Availability of data and materials
Not applicable.

Competing interests
The authors declare that they have no competing interests

Received: 1 September 2019 Accepted: 6 April 2020
Published online: 26 May 2020

References

1. Antonino-Daviu J, Climente-Alarcon V, Tsoumas I, Georgoulas G, Pérez RB (2013) Multi-harmonic tracking for diagnosis of rotor asymmetries in wound-rotor induction motors. In: IECON 2013: Proceedings of 39th annual conference of the industrial electronics society, pp 5555–5560
2. Antonino-Daviu J, Quijano-López A, Climente-Alarcon V, Garín-Abellán C (2017) Reliable detection of rotor winding asymmetries in wound rotor induction motors via integral current analysis. IEEE Trans Ind Appl 53(3):2040–2048
3. Athulya K (2018) Inter Turn Fault Diagnosis in Wound Rotor Induction Machine Using Wavelet Transform. In: IC4 2018: proceedings of international CET conference on control, communication, and computing (IC4), pp 22–27
4. Climente-Alarcon V, Riera-Guasp M, Antonino-Daviu J, Roger-Folch J, Vedreño-Santos F (2012) Diagnosis of rotor asymmetries in wound rotor induction generators operating under varying load conditions via the Wigner-Ville Distribution. In: SPEEDAM 2012: Proceedings of IEEE international symposium on power electronics, electrical drives, automation and motion, pp 1378–1383
5. Duvvuri S (2018) Modeling and simulation of slip-ring induction motors with stator and rotor inter-turn faults for diagnostics. In: IICPE 2018: Proceedings of 8th IEEE India international conference on power electronics
6. Gritli Y, Rossi C, Casadei D, Filippetti F, Bellini A, Capolino G-A (2017) A diagnostic space vector-based index for rotor electrical fault detection in wound-rotor induction machines under speed transient. IEEE Trans Ind Electron 64(5):3892–3902
7. Kowalski CT, Orlowska-Kowalska T (2003) Neural networks application for induction motor faults diagnosis. Math Comput Simul 63(3):435–448
8. Leung WS, Ma WF (1967) Investigation of induction motors with unbalanced secondary winding connections. Proc Inst Electr Eng 114(7):974–977
9. Ma WF, Leung AWS (1969) Abnormal operation of induction motors with two-phase rotors. Int J Electr Eng Educ 7:193–197
10. Naderi P, Taheri A (2015) Slot numbering and distributed winding effects analysis on the torque/current spectrum of three-phase wound-rotor induction machine using discrete modeling method. Electr Power Compon Syst 43(15):1717–1726
11. Naderi P, Shiri A (2017) Rotor/stator inter-turn short circuit fault detection for saturable wound-rotor induction machine by modified magnetic equivalent circuit approach. IEEE Trans Magn 53(7):1–13
12. Roshanfekr R, Jalilian A (2015) Analysis of rotor and stator winding inter-turn faults in WRIM using simulated MEC model and experimental results. Electr Power Syst Res 119:418–424
13. Roshanfekr R, Jalilian A (2018) An approach to discriminate between types of rotor and stator winding faults in wound rotor induction machines. In: ICEE2018: Proceedings of 26th Iranian conference on electrical engineering, pp 1067–1070
14. Salah A, Youguang G, Dorrell D (2016) Impedance matrix analysis technique in wound rotor induction machines including general rotor asymmetry. In: IECON 2016: Proceedings of the 42nd annual conference of the IEEE industrial electronics society, pp 1821–1826
15. Subhasis N, Toliyat HA, Xiaodong Li (2005) Condition monitoring and fault diagnosis of electrical motors-a review. IEEE Trans Energy Convers 20(4):719–729
16. Tiegna H, Amara Y, Barakat G (2013) New line-starting method of a class of synchronous motors. In: IEMDC 2013: proceedings of IEEE international electric machines and drives conference, pp 1471–1476
17. Tsoumas IP, Georgoulas G, Antonino-Daviu J (2017) On the detectability of rotor asymmetries in induction motors from the start-up transient. In: SDEMPED 2017: proceedings of IEEE 11th international symposium on diagnostics for electrical machines, power electronics and drives, pp 31–37
18. Yeh CC et al (2008) A reconfigurable motor for experimental emulation of stator winding interturn and broken bar faults in polyphase induction machines. IEEE Trans Energy Convers 23(4):1005–1014

Publisher's Note